ChemComm

COMMUNICATION

View Article Online
View Journal | View Issue

Open Access Article. Published on 15 October 2015. Downloaded on 9/22/2024 12:03:33 PM.
This article is licensed under a Creative Commons Attribution 3.0 Unported Licence.

Cite this: *Chem. Commun.*, 2016, **52**, 9028

Received 15th September 2015,
Accepted 9th October 2015

DOI: 10.1039/c5cc07732j

www.rsc.org/chemcomm

Fast microwave treatments of single source alkoxides for nanostructured Li-ion battery electrodes†

Josefa Vidal Laveda,[a] Vibhuti Chandhok,[a] Claire A. Murray,[b] Gary W. Paterson[c] and Serena A. Corr*[a]

Microwave or ultrasonic treatment of metal alkoxides presents a fast, low cost route to both anode and cathode nanomaterials for Li-ion battery applications. Here, we demonstrate the formation of LiMPO$_4$ (M = Fe, Mn) and Mn$_3$O$_4$ nanostructures *via* this simple route which exhibit excellent electrochemical performances. This approach opens up a new avenue for the targeted design of nanostructured materials, where co-location of the desired metals in a single starting material shortens reaction times and temperatures since there is a decrease in diffusional energy requirements usually needed for these reactions to proceed.

Control over the design of inorganic nanostructures of preferred crystal structure, particle size and morphology is highly desirable and challenges remain in achieving this in a reliable and reproducible manner. There are continuous research efforts to obtain electrode materials for use in Li-ion batteries with high energy densities to satisfy the increasing need for long lasting energy storage devices.[1] Amongst the positive insertion electrodes, olivine-structured lithium transition metal phosphates such as LiFePO$_4$ have been recognized as low cost, non-toxic, safe alternatives to layered LiCoO$_2$ showing good thermal stability, high specific charge capacity ($\sim$170 mA h g^{-1}) and good cyclability.[2] Crystalline LiMPO$_4$ (M = Fe or Mn) has an orthorhombic unit cell in which O^{2-} ions form strong covalent bonds with P^{5+} to form PO$_4^{3-}$ tetrahedral units stabilizing the entire network, assuring stable operation at high temperatures. Nanostructured insertion electrodes are of particular interest due to the potential improvements in cycling performance, as smaller sizes allow shorter path lengths for the Li-ions to diffuse, while the increased surface areas enhance electrode–electrolyte interactions.[3] Also of interest is the possibility of partial substitution of Fe^{2+} with Mn^{2+} in the olivine structure to afford mixed metal LiFe$_{1-x}$Mn$_x$PO$_4$ phosphates with increased redox potential due to the higher Mn$^{2+/3+}$ potentials compared to the Fe$^{2+/3+}$ pair (3.45 V *vs.* Li$^+$/Li^0 for LiFePO$_4$ and 4.10 V *vs.* Li$^+$/Li^0 for LiMnPO$_4$).[4] Therefore, there exist many opportunities to improve the behaviour and electrochemical performance of nanostructured electrode materials, beginning with careful consideration of the synthesis route employed. In the case of anode materials, metal oxides are finding increasing use as alternatives to graphite for negative electrodes in Li-ion batteries. Since transition metal oxides can react with more than one Li per transition metal atom, exceptionally high specific capacities are theoretically possible.[5] However, the low electronic conductivity and large volume expansion associated with these materials often lead to poor cycling performance. Drastic volume variations during charging/discharging can cause disintegration of the electrode. Amongst several metal oxides, Mn$_3$O$_4$ is an attractive candidate for use as an anode material due to the high abundance of Mn, its environmental benignity and low cost.[6] Furthermore, electrochemical studies of Mn$_3$O$_4$ nanostructures have shown that decreasing the particle size markedly reduces the polarization displayed by the electrodes and improves the reversibility of the cycling process and the rate capability. For example, Luo *et al.* demonstrated that a carbon nanotube–Mn$_3$O$_4$ composite displayed a reversible capacity of 1912.9 mA h g^{-1} for 10 nm particles compared to 367 mA h g^{-1} for 165 nm Mn$_3$O$_4$ particles.[7] Increased capacities can also be realised through the use of conductive coatings such as reduced graphene oxide and the growth of porous or hollow morphologies.[6,8,9,10]

Often, routes to exotic morphologies or nanostructured particles can be time consuming and non-trivial. Fast, low temperature syntheses are therefore highly desirable for the preparation of high quality functional inorganic nanoparticles. Compared to conventional solid state reactions which often require high temperatures and long reaction times, syntheses employing microwave or ultrasonic irradiation can provide relatively low temperature routes to desired crystal structures that generally offer a significant reduction in reaction times and energy consumption.[11–13] Our efforts have led us to develop a

---

[a] *School of Chemistry, University of Glasgow, Glasgow G12 8QQ, UK. E-mail: serena.corr@glasgow.ac.uk; Tel: +44 (0)141 3302274*
[b] *Diamond Light Source, Didcot, Oxfordshire, OX11 0DE, UK*
[c] *School of Physics and Astronomy, University of Glasgow, Glasgow G12 8QQ, UK*

† Electronic supplementary information (ESI) available. See DOI: 10.1039/c5cc07732j

This journal is © The Royal Society of Chemistry 2016

Open Access Article. Published on 15 October 2015. Downloaded on 9/22/2024 12:03:33 PM.
This article is licensed under a Creative Commons Attribution 3.0 Unported Licence.

series of metalorganic precursors which provide an additional advantage for decreased reaction times and temperatures. Metal alkoxides have previously been employed as excellent starting materials for metal oxide thin films.[14] The attractiveness of a heterometallic alkoxide as a starting material lies in their easy thermal decomposition and in the possibility of having, in a single compound, more than one of the desired metals with a known stoichiometry. Co-location of several metals in these precursors bypasses the need of diffusional mixing and could afford highly crystalline materials through a less energy consuming process. Here, we demonstrate the versatility of this approach for the clean preparation of both positive and negative electrodes for Li-ion batteries through relatively fast and low temperature microwave and ultrasound-assisted methods. Furthermore, electrochemical testing reveal the excellent performance of these nanostructures, establishing this synthetic approach as one to yield high performance electrode materials across the olivines and metal oxides.

Initially, the previously reported metal alkoxide $[Fe(O^tBu)_2(THF)]_2$ and a new, similarly synthesized Mn alkoxide were employed as precursors for the preparation of olivine structured positive electrodes $LiMPO_4$ (M = Fe and Mn) and the hausmannite structured negative electrode Mn_3O_4, according to Fig. 1. In the case of the olivine nanostructures, powder products were obtained after only ten minutes of microwave treatment. For the formation of Mn_3O_4, a hydrolysis route promoted by ultrasonic irradiation was used. Previous reports have demonstrated that hydrolysis of the metal alkoxide $[Fe(O^tBu)_2(THF)]_2$ yields magnetite nanocrystals.[15] In the current work, the Mn alkoxide analogue has been prepared for the first time and hydrolysed under ultrasonic treatment at room temperature to afford nanostructured Mn_3O_4. High resolution powder X-ray diffraction (XRD) measurements of the $LiFePO_4$ and $LiMnPO_4$ samples obtained at the I11 beamline at Diamond Light Source reveal phase-pure materials crystallised in the orthorhombic *Pnma* space group. The slight shifting of the peaks towards lower angles for $LiMnPO_4$ is a signature of the larger cation size of Mn^{2+} in comparison to Fe^{2+}. Powder XRD data were fit by Rietveld analysis, with excellent agreement to the *Pnma* model obtained.

In order to establish this alkoxide route as applicable for the preparation of a range of $LiFe_{1-x}Mn_xPO_4$ materials, stoichiometric amounts of the individual Fe and Mn alkoxides were reacted following the same procedure to prepare $LiFe_{0.5}Mn_{0.5}PO_4$. However, analysis of the resulting powder XRD pattern reveals a mixture of $LiFe_{0.5}Mn_{0.5}PO_4$ and Fe_3O_4 magnetite is obtained (Fig. S1, ESI†). In an effort to avoid impurities, a bimetallic alkoxide with a suggested formula "$[Fe_{0.5}Mn_{0.5}(O^tBu)_2(THF)]_2$" was prepared and used as a starting material. We suggest this formula according to our synthesis, but as yet we have not obtained a single crystal of sufficient quality to elucidate the crystal structure. Further efforts to characterise this compound are currently underway. However, we are confident that this route does not simply produce a mixture of the previous Fe- and Mn-alkoxides since the use of this proposed alkoxide to prepare $LiFe_{0.5}Mn_{0.5}PO_4$ using the same conditions as Fig. 1 affords single phase products. Rietveld refinements of the high resolution powder XRD data shown in Fig. 2(b) indicates that phase pure $LiFe_{0.5}Mn_{0.5}PO_4$ was obtained, with no evidence of any impurities. Table S1 (ESI†) summarises the calculated lattice parameters for the different olivines. In the case of the ultrasonic treatment of the "$[Mn(O^tBu)_2(THF)]_2$" precursor, a brown powder was obtained which, when characterised with XRD, could be fit to a $I4_1/amdZ$ space group, confirming phase pure Mn_3O_4 hausmannite (Fig. S2, ESI†). SEM images of the $LiFePO_4$ sample revealed non-uniform platelets, with sizes ranging from 50 to 250 nm. Elongated particles were obtained for $LiFe_{0.5}Mn_{0.5}PO_4$, with rod-like particles found for $LiMnPO_4$. This highlights the strong influence of the Mn content on the resulting particle morphology and size. The fringes visible in TEM images of the $LiFe_{1-x}Mn_xPO_4$ (x = 0, 0.5 and 1) samples (Fig. S3, ESI†) reveal the samples are crystalline and lattice spacings are consistent with the planes indicated the images.[16] The insets are Fourier transforms of

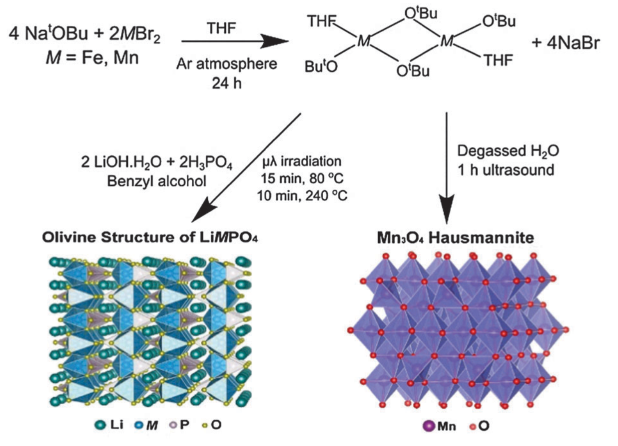

Fig. 1 Reaction schematic for the synthesis of $LiMPO_4$ (M = Fe or Mn) and Mn_3O_4 using metal alkoxide precursors.

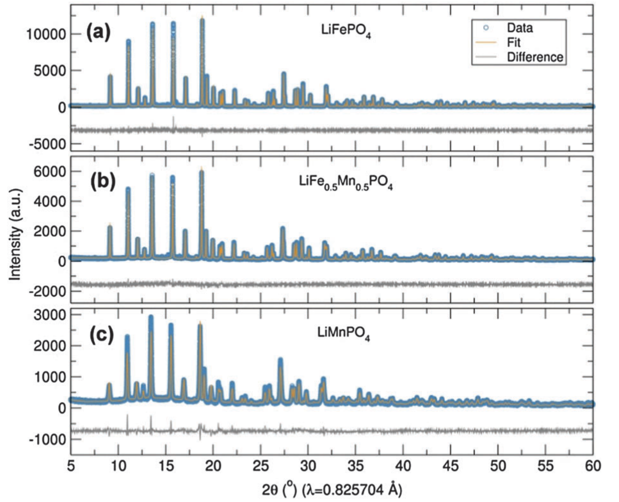

Fig. 2 Rietveld analysis of XRD data of (a) $LiFePO_4$, (b) $LiFe_{0.5}Mn_{0.5}PO_4$ and (c) $LiMnPO_4$ nanostructures prepared from $[Fe(O^tBu)_2(THF)]_2$, "$[Fe_{0.5}Mn_{0.5}(O^tBu)_2(THF)]_2$" and "$[Mn(O^tBu)_2(THF)]_2$" alkoxides, respectively.

Open Access Article. Published on 15 October 2015. Downloaded on 9/22/2024 12:03:33 PM. This article is licensed under a Creative Commons Attribution 3.0 Unported Licence.

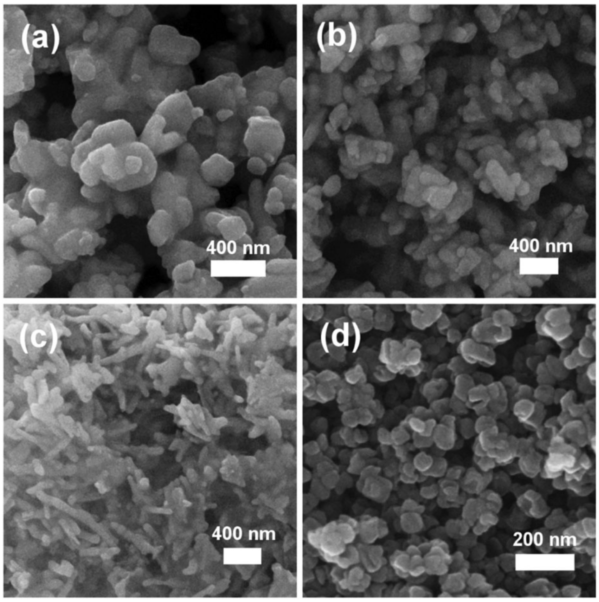

Fig. 3 SEM images of (a) $LiFePO_4$, (b) $LiFe_{0.5}Mn_{0.5}PO_4$, (c) $LiMnPO_4$ and (d) Mn_3O_4 nanostructures prepared from metal alkoxide precursors.

the TEM images. Indexing of the patterns reveals the crystal long-axes, indicated by the green lines in the images, lie within a few degrees of the [101], [020] and [112] axes for $LiMnPO_4$, $LiFePO_4$ and $LiFe_{0.5}Mn_{0.5}PO_4$, respectively. Fig. 3(d) reveals quasi-spherical Mn_3O_4 nanoparticles with a typical size of 80 nm.

Galvanostatic cycling at room temperature of the $LiFePO_4$ sample was conducted over the voltage range of 2.2 to 4.0 V at a C/20 rate in a Swagelok cell-type. To enhance the electronic conductivity, a simple carbon coating using sucrose was performed, as poor electron mobility will limit the Li^+ extraction/insertion. From the voltage-composition plot (Fig. S4, ESI†) it can be observed that approximately 0.6 Li^+ were reversibly extracted during the cycling process. It is well established that the major $LiFePO_4$ capacity is attributed to the Li^+ insertion/extraction process from the $LiFePO_4$ particles ($LiFePO_4 \rightleftharpoons FePO_4 + Li^+ + e^-$). The two main limiting factors reported for why Li-ions cannot be fully deinserted from the ordered-olivine structure are: limited Li^+ phase-boundary diffusion and the low electronic conductivity during the charge/discharge processes. For example, Li^+ diffusion can be blocked by ionic disorder, foreign phases or stacking faults, impeding the reversible $LiFePO_4/FePO_4$ phase transformation.[17] The representative charge and discharge voltage profile for the $LiFePO_4$ nanoparticles obtained through microwave-treatment of the alkoxide precursor shown in Fig. 4(a) indicates that charge and discharge capacities of approximately 150 mA h g^{-1} were obtained, close to the theoretical capacity of this material (170 mA h g^{-1}). Furthermore, there is almost no capacity fading over at least 20 cycles [inset, Fig. 4(a)]. The rate behaviour of the C/$LiFePO_4$ and the C/$LiFe_{0.5}Mn_{0.5}PO_4$ phases was also investigated in order to examine the rate capabilities as a function of Mn content and particle morphology (see also Fig. S5, ESI†). Fig. 4(b) shows that the discharge capacities of the C/$LiFePO_4$ and C/$LiFe_{0.5}Mn_{0.5}PO_4$ phases decrease with higher C rates. This effect is more pronounced for the $LiFePO_4$ sample. High C rates up to 10C delivered discharge capacities of 75 mA h g^{-1} and 50 mA h g^{-1} for the C/$LiFe_{0.5}Mn_{0.5}PO_4$ and C/$LiFePO_4$ phases, respectively.

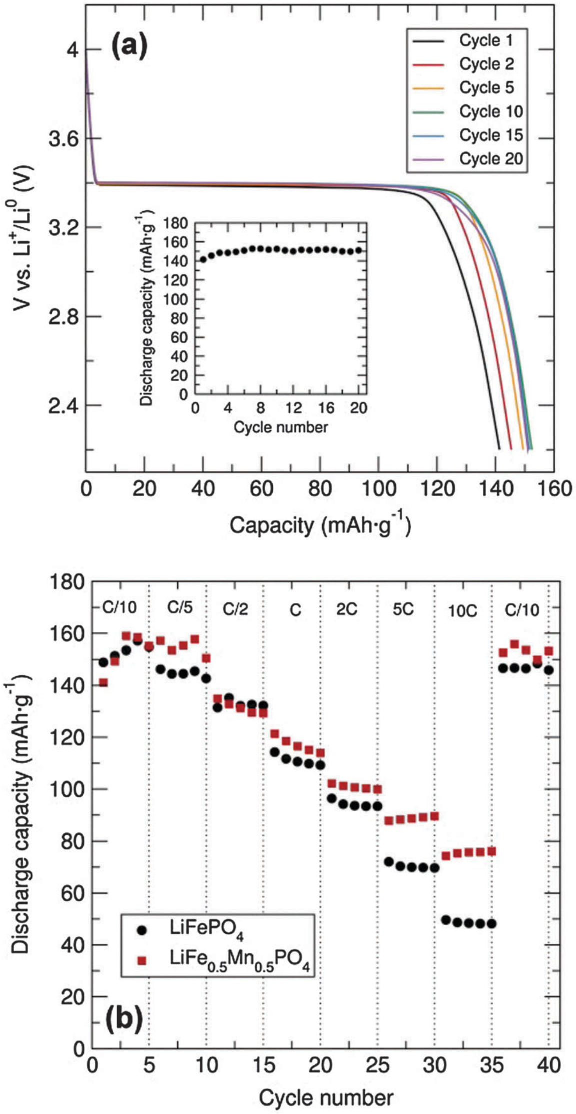

Fig. 4 (a) Cycling performance and capacity fading (inset) of C/$LiFePO_4$ prepared from $[Fe(O^tBu)_2(THF)]_2$ alkoxide precursor (mixed with C black and PTFE in 60 : 30 : 10 weight%) between 2.2 and 4.0 V at C/20 rate. (b) Rate performance of C/$LiFePO_4$ and C/$LiFe_{0.5}Mn_{0.5}PO_4$ (mixed with C black and PTFE in 60 : 30 : 10) at different charge–discharge C rates.

The C/$LiFe_{0.5}Mn_{0.5}PO_4$ presented here showed an improved rate capability at 10C in comparison to the ~55 mA h g^{-1} at 8C reported previously for $LiFe_{0.5}Mn_{0.5}PO_4$ prepared *via* an electrospun synthetic procedure.[18] Moreover, it must be noted that in both cases here our capacity was recovered when cycling back to C/10 rate after increasingly faster rates. These results suggest that partial substitution of Fe^{2+} by Mn^{2+} in the olivine structure affords a noticeable enhancement in the rate capability of these electrodes. The observed improvement in the electrochemical performance of the C/$LiFe_{0.5}Mn_{0.5}PO_4$ material in comparison to C/$LiFePO_4$ could also be attributed to the

Open Access Article. Published on 15 October 2015. Downloaded on 9/22/2024 12:03:33 PM. This article is licensed under a Creative Commons Attribution 3.0 Unported Licence.

decrease in particle size. XRD characterization of the cycled materials in the discharge state showed that the extraction/insertion process did not affect the structure of the C/$LiFePO_4$ and the C/$LiFe_{0.5}Mn_{0.5}PO_4$ composites (Fig. S6 and S7, ESI†), confirming the good structural stability of these positive insertion electrodes upon cycling. Cyclic voltammetry (CV) measurements of the C/$LiFePO_4$ and the C/$LiFe_{0.5}Mn_{0.5}PO_4$ composites were performed at a scan rate of 0.1 mV s^{-1} between 2.5 and 4.5 V and demonstrated good electrochemical reversibility (Fig. S8, ESI†). Electrochemical measurements of C/Mn_3O_4 at a current density of 100 mA h g^{-1} over a 0.01–3.00 V range revealed an initial discharge capacity of ~3200 mA h g^{-1} that sharply decreased to approximately 1300 mA g^{-1} at the second cycle (Fig. S9, ESI†). It must be remarked that this initial discharge capacity of the C/Mn_3O_4 composite was significantly larger than previous reports.[19–22] The large capacity drop after the first cycle could be attributed to irreversible processes such as solid electrolyte interface formation and electrolyte decomposition. Fig. S7 (ESI†) shows a drastic decrease in the capacity with cycling but a discharge capacity of 460 mA h g^{-1} is still reached at the 20th cycle. Lack of Bragg diffraction peaks in the XRD patterns of the cycled C/Mn_3O_4 material suggests degradation, possibly due to significant volume changes (Fig. S10 and S11, ESI†). Studies are currently underway to try to alleviate this breakdown through surface coatings. CV shows good peak overlap after the first cycle, confirming the good cycling reversibility (Fig. S12, ESI†). An intense cathodic peak at around 0.3 V and an anodic peak at approximately 1.4 V were observed. The possible formation of a solid electrolyte interface and/or electrolyte decomposition during the first charge/discharge cycle is confirmed from the difference observed in the first discharge CV curve.

We have presented a low cost and green synthetic approach for the preparation of metal alkoxides to be used as precursors in the synthesis of phase pure olivine nanostructured $LiFe_{1-x}Mn_xPO_4$ (x = 0, 0.5 and 1) and Mn_3O_4 hausmannite nanocrystals through fast microwave and ultrasound-assisted routes, respectively. Moreover, we have demonstrated the versatility of these metal alkoxide precursors for the synthesis of both cathode and anode materials for Li-ion batteries. Electrochemical testing of $LiFePO_4$ and $LiFe_{0.5}Mn_{0.5}PO_4$ samples revealed excellent cyclability with charge/discharge capacities close to theoretical values (~155 mA h g^{-1} *vs.* 170 mA h g^{-1} at C/20 rate). These positive insertion electrodes also displayed rate capabilities comparable to the best performing olivine-structured metal phosphates in the literature, suggesting the suitability of the metal alkoxide precursors presented here in the generation of high quality olivine mixed-metal phosphates *via* a fast microwave-assisted synthesis. Further improvements in the carbon coating of our metal oxide nanoparticles synthesised by a straightforward room temperature ultrasound-assisted synthesis could dramatically enhance the battery cycling performance. Our future work will concentrate on the preparation of heterometallic alkoxides containing both Li and the desired transition metal in a single precursor in an effort to obtain highly crystalline nanostructures with excellent battery performance in a single step.

The authors gratefully acknowledge the allocation of beamtime at the I11 beamline at the Diamond Light Source. This work was supported by funding from the EPSRC (EP/K026290/1 and EP/N001982/1). We thank the School of Chemistry at the University of Glasgow for PhD funding and support.

Notes and references

1 J.-M. Tarascon and M. Armand, *Nature*, 2001, 414; B. Kang and G. Ceder, *Nature*, 2009, 458.
2 H. Liu, F. C. Strobridge, O. J. Borkiewicz, K. M. Wiaderek, K. W. Chapman, P. J. Chupas and C. P. Grey, *Science*, 2014, **344**, 6191.
3 A. Manthiram, A. Vadivel Murugan, A. Sarkar and T. Muraliganth, *Energy Environ. Sci.*, 2008, **1**, 621.
4 V. Aravindan, J. Gnanaraj, Y.-S. Lee and S. Madhavi, *J. Mater. Chem. A*, 2013, **1**, 3518.
5 H. Kim, D.-H. Seo, H. Kim, I. Park, J. Hong, K.-Y. Park and K. Kang, *Chem. Mater.*, 2012, **24**, 720.
6 H. Wang, L.-F. Cui, Y. Yang, H. Sanchez Casalongue, J. Tucker Robinson, Y. Liang, Y. Cui and H. Dai, *J. Am. Chem. Soc.*, 2010, **132**, 13978.
7 S. Luo, H. Wu, Y. Wu, K. Jiang, J. Wang and S. Fan, *J. Power Sources*, 2014, **249**, 463.
8 C. Chen, H. Jian, X. Fu, Z. Ren, M. Yan, G. Qian and Z. Wang, *RSC Adv.*, 2014, **4**, 5367.
9 J. Yue, X. Gu, L. Chen, N. Wang, X. Jiang, H. Xu, J. Yang and Y. Qian, *J. Mater. Chem. A*, 2014, **2**, 17421.
10 Z. Bai, X. Zhang, Y. Zhang, C. Guo and B. Tang, *J. Mater. Chem. A*, 2014, **2**, 16755.
11 Y. Luo, S. Fan, N. Jao, S. Zhong and W. Liu, *Dalton Trans.*, 2014, **43**, 15317.
12 I. Bilecka, A. Hintennach, I. Djerdj, P. Novák and M. Niederberger, *J. Mater. Chem.*, 2009, **19**, 5125; I. Bilecka, A. Hintennach, M. D. Rossell, D. Xie, P. Novák and M. Niederberger, *J. Mater. Chem.*, 2011, **21**, 5881; T. E. Ashton, J. Vidal Laveda, D. A. MacLaren, P. J. Baker, A. Porch, M. O. Jones and S. A. Corr, *J. Mater. Chem. A*, 2014, **2**, 6238.
13 F. Yu, L. Zhang, M. Zhu, Y. An, L. Xia, X. Wang and B. Dai, *Nano Energy*, 2014, **3**, 64.
14 M. Mantymaki, M. Ritala and M. Leskela, *Coord. Chem. Rev.*, 2012, **256**, 854.
15 G. B. Biddlecombe, Y. Guńko, J. M. Kelly, S. C. Pillai, J. M. D. Coey, M. Venkatesan and A. P. Douvalis, *J. Mater. Chem.*, 2001, **11**, 2937; S. A. Corr, Y. K. Gun'ko, A. P. Douvalis, M. Venkatesan and R. D. Gunning, *J. Mater. Chem.*, 2004, **14**, 944; S. A. Corr, Y. Guńko, A. P. Douvalis, M. Venkatesan, R. D. Gunning and P. D. Nellist, *J. Phys. Chem. C*, 2008, **112**, 1008.
16 G. Qin, S. Xue, Q. Maa and C. Wang, *CrystEngComm*, 2014, **16**, 260.
17 L.-H. Hu, F.-Y. Wu, C.-T. Lin, A. N. Khlobystov and L.-J. Li, *Nat. Commun.*, 2013, **4**, 1687.
18 R. von Hagen, H. Lorrmann, K.-C. Möller and S. Mathur, *Adv. Energy Mater.*, 2012, **2**, 553.
19 H. Huang, L. Zhang, Y. Xia, Y. Gan, X. Tao, C. Liang and W. Zhang, *New J. Chem.*, 2014, **38**, 4743.
20 J. Gao, M. A. Lowe and H. D. Abruña, *Chem. Mater.*, 2011, **23**, 3223.
21 Y. Liu, W. Wang, Y. Wang, Y. Ying, L. Sun and X. Peng, *RSC Adv.*, 2014, **4**, 16374.
22 I. Nam, N. D. Kim, G.-P. Kim, J. Park and J. Yi, *J. Power Sources*, 2013, **244**, 56.